Journal of Materials Chemistry A

ROYAL SOCIETY OF CHEMISTRY

PAPER

View Article Online
View Journal



Cite this: DOI: 10.1039/d6ta00284f

# Designing recyclable inorganic–organic hybrid polymer coatings through integrating silicone-based molecular scission points

Christopher Fischer, *[ab] Anja Hart,[a] Ferdinand Somorowsky, [a] Claudia Stauch, [a] Diana Lau, [a] Gerhard Sextl[ab] and Joseph C. Furgal *[c]

Received 11th January 2026
Accepted 31st March 2026

DOI: 10.1039/d6ta00284f

rsc.li/materials-a

Inorganic–organic hybrid polymer coatings (IOHPCs) enhance the sustainability and the quality of life during their use *e.g.*, as PFAS-free hydrophobic coatings on glass surfaces. Although their modular structure is key to highly adaptable performance, it poses an environmental challenge because it hinders efficient recycling. This study fundamentally shifts the molecular design paradigm of IOHPCs to achieve harmony between performance and recyclability (Design for Recycling). Therefore, silicone chains are introduced as molecular scission points within IOHPCs to enable fluoride-triggered depolymerization. The resulting coatings exhibited hydrophobic surfaces and tunable mechanical properties (full range of pencil hardness from very soft to very hard) that depended on silicone chain length and concentration. Contact with the tetrabutylammonium fluoride (TBAF) catalyst induced the collapse of the hybrid network and total delamination in a single step. This process yields reusable outputs, such as cyclic siloxanes (mainly $D_4$), suitable for silicone synthesis, and also preserves the substrate for direct reuse. These results demonstrate that recyclability can be successfully incorporated into the molecular design of IOHPCs, thereby making them compatible with existing silicone recycling techniques while preserving their coating performance.



## Introduction

Global plastic production was 400 million tonnes in 2022, of which approximately 34% were incinerated and 40% were landfilled, while only 9% were recycled.[1] It is forecast that total plastic waste will reach 12 000 million tonnes by 2050, underscoring the need to improve recycling rates to avoid drastic effects on resource depletion, human health, and the environment.[2,3] One reason for low plastic recycling rates is that products consist of multi-material combinations whose heterogeneous structure makes recycling inherently difficult.[4–6] This challenge is amplified by the fact that these materials are designed with the aim to achieve specific performance profiles in use, rather than to facilitate post-lifecycle recycling.[7,8] Examples include laminated plastics, coated materials and composites containing plastics, ceramics, metals, as well as hybrid materials in which different material parts are covalently bonded. In cases where recycling solutions exist, they are still on a laboratory scale and are not yet economically feasible.[6,9–11]

Inorganic–organic hybrid polymer coatings (IOHPCs) fall into both the category of coated materials and the category of hybrid polymers. On the one hand, in-use IOHPCs significantly contribute to today's life quality by serving applications as PFAS-free hydrophobic, corrosion-inhibiting, bronze conservation in the outdoor environment, and oxygen barrier coatings for packaging materials.[12–17] However, post-lifecycle, they pose a potential environmental threat as waste, as the recycling of IOHPCs is inherently challenging due to their combination of diverse material types in a single compound. In contrast to composite materials, in IOHPCs inorganic and organic elements of the coating's hybrid polymer matrix are not only combined physically but are covalently bonded.[18,19] Generally, the inorganic network is derived from alkoxysilanes, such as $Si(OR)_4$ (R = ethoxy or methoxy), which provide rigidity, thermal stability, and mechanical strength. The organic network often consists of polymer-like units and is covalently bonded to the inorganic network *via* functional organosilanes, $SiR'(OR)_3$ (R = ethoxy or methoxy, R′ can refer, for example, to amino- or epoxy-functionalization). These structures allow for the integration of organic groups R′ into the hybrid material and implement flexibility, processability, and tunability of surface properties, such as the surface polarity ranging from hydrophilic to hydrophobic.[19–22] While advantageous for performance, this lack of homogeneity poses significant obstacles for recycling. Thus, the common solution so far is to reduce the coating

[a]Fraunhofer Institute for Silicate Research, Neunerplatz 2, 97082 Würzburg, Germany. E-mail: christopher.fischer@isc.fraunhofer.de
[b]University of Würzburg, Department of Chemical Technology of Materials Synthesis, Röntgenring 11, 97070 Würzburg, Germany
[c]Department of Chemistry and Center for Photochemical Sciences, Bowling Green State University, Ohio 43403, USA. E-mail: furgalj@bgsu.edu

thickness as much as possible (<1–4 μm) to minimize the coating's share of foreign material mass in substrate recycling streams.[23] However, with increasing number of recycling loops this strategy often leads to downcycling.[24–28]

To move towards a truly circular solution, a fundamentally different paradigm is required, where functional materials are designed with an intrinsic harmony between in-use performance and post-lifecycle transformation.[4] This principle is commonplace in nature, where post-lifecycle functionality is already implemented at the design stage. A walnut shell for instance, provides mechanical protection during growth yet opens along predetermined scission points to enable sprouting, just like leaves are performing photosynthesis during summer and later detach at predetermined scission points in fall.[29,30] This natural paradigm of coupling function with designed disassembly inspired our approach. We thus translated this principle to the structural design of IOHPCs on the molecular level and implemented chemically triggered molecular scission points within IOHPCs to implement a design for recycling.[4,31,32] In detail, we aimed to develop IOHPCs that can be efficiently degraded into reusable synthons, enabling the gentle delamination and subsequent reuse of valuable substrate materials.

For choosing the optimal designed molecular scission point, we drew inspiration from advances in the recent development of new depolymerization techniques and recycling methods developed for silicone-based materials at low temperatures (20–180 °C).[33–38] Herein, the aim is the reduction of energy consumption towards conventional methods requiring medium (180–350 °C) or high temperatures (350–550 °C).[39,40] Thus, a variety of depolymerization agents, including gallium-catalyzed systems in combination with boron trichloride, polydentate ligand–potassium silanolate systems using crown ethers as ligands, tetrabutylammonium difluorotriphenylsilicate (TBAT), as well as tetrabutylammonium fluoride (TBAF), that enable the depolymerization to reusable synthons (chlorosilanes or cyclodiorganopolysiloxanes) at low temperatures have been investigated.[33–37,41] Especially, the at RT reactive TBAF method is of great economic and ecological interest due to cost effectiveness, low catalyst loadings and solvent reuse.[34,41] In more detail, catalytic amounts of TBAF were used to depolymerize PDMS chains into cyclic siloxanes of four, five, or six units ($D_4$, $D_5$, and $D_6$). Those cyclic structures are industrially used as educts for the synthesis of linear silicones, elegantly closing the loop for silicone materials, as shown in Scheme 1.[33,34,40,41] Another argument for choosing silicones as the molecular scission point is their stability toward different weathering conditions, contributing to avoiding unintended decomposition.[42,43]

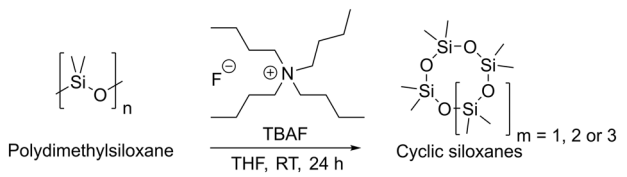


Scheme 1 Depolymerization of polydimethylsiloxane using tetrabutylammonium fluoride. Depolymerization products are $D_4$, $D_5$, and $D_6$.

The primary focus of this study is the integration of silicone chains into the IOHPC matrix as molecular scission points to make it amenable to a subsequent mild and sustainable recycling processes. An essential aspect here is to achieve a balance between functional performance (*e.g.*, transparency, hydrophobicity, or hardness) and recyclability of the coatings by targeted parameter variation (*e.g.*, silicone chain length and content). In addition, the coating-substrate delamination process to enable complete substrate recovery and reuse was evaluated.

# Experimental

### Materials and methods

All reagents and solvents were used without further purification. Silicone oil with a weight-average molecular weight $M_w$ of 550 Da was purchased from Sigma-Aldrich (MO, USA), and with a weight-average molecular weight $M_w$ of 3400 Da was a gift from Genesee Polymer Corporation (MI, USA). The suppliers for dibutyltin dilaurate (DBTL) and tetramethylammonium hydroxide (TMAH) were Sigma-Aldrich (MO, USA). Calcium chloride ($CaCl_2$) was purchased by Carl Roth GmbH & Co. KG (Lauda-Königshofen, Germany). Microscope slides were supplied by Paul Marienfeld GmbH & Co. KG (Lauda-Königshofen, Germany) and steel substrates (DC04) by Rocholl GmbH (Eschelbronn, Germany). Tetrahydrofuran (THF) and ethyl acetate (EtOAc) were purchased from Millipore-Sigma (MO, USA). Methyl ethyl ketone was purchased from Sigma-Aldrich (MO, USA). Tetrabutylammonium fluoride (TBAF) was purchased from Acros Organics (MA, USA). (3-Glycidyloxypropyl)trimethoxysilane (GPTMS), 3-aminopropyltriethoxysilane (APTES), and tetraethyl orthosilicate (TEOS) were purchased from Gelest Inc. (PA, USA). Ciba® ORASOL® Blue CN (Cu-phthalocyanine base) was purchased from Ciba Specialty Chemicals Inc. (Basel, Switzerland).

### Coating synthesis and coating procedure

The silane precursors (GPTMES, TEOS) and the hydroxy-terminated polydimethylsiloxane (PDMS-OH, $M_w$ 550 or 3400 Da) were mixed until dissolution in methyl ethyl ketone (MEK). Subsequently, 3.6 wt% of a 10 wt% DBTL/MEK solution was added to the mixture and stirred for 5 minutes at RT. Then, APTES was added, and the reaction mixture was stirred for 70 minutes at RT, while the viscosity significantly increased. The molar ratios of GPTMS, TEOS, and APTES were all set to 1, while the silicone concentration ranged from 4–20 mol%. Selected coatings were coloured with Ciba® ORASOL® Blue CN (Cu-phthalocyanine base) for display purposes. Prior to coating, each substrate was thoroughly cleaned with acetone. Additionally, steel substrates were pre-treated *via* $SiO_x$ to enhance adhesion and wetting (see $SiO_x$ pre-treatment for details). After that, the reaction mixture was flooded onto different substrates (*e.g.*, glass slides, polyolefin, aluminum and stainless steel) by soaking approximately 1 g of the reaction mixture in a plastic

pipette and then spreading it evenly over the substrates. Coatings cured within 45 minutes at ambient conditions. However, a post-curing step was conducted at 130 °C for 1 hour under ambient atmosphere.

### $SiO_x$ pre-treatment

Steel substrates were pre-treated with a flame-sprayed silica coating ($SiO_x$ pre-treatment). Therefore, a fuel gas–air mixture contains small amounts of a silane component. A silicate is produced in an open flame and deposited on the substrate surface as a thin silicate layer. Two flame treatments were carried out at 90° to each other on each substrate.

### Depolymerization trials

For analytical purposes, a bulk sample of the IOHPC (0.5 g) was submerged in 5 mL of EtOAc or THF. Afterward, 0.2 mL of a 1 M TBAF solution in THF was added, and the mixture was stirred overnight at RT. The resulting mixture contained a clear solution and a precipitate. The components were separated by centrifugation and washed with EtOAc or THF trice. The clear solution containing cyclic siloxane products was quenched with an excess of $CaCl_2$ overnight to quench free fluoride. $CaCl_2$ and $CaF_2$ were removed *via* centrifugation and decantation.

### Delamination trials

The coated substrate (steel, glass, plastic, or aluminum) was submerged in 20 mL of THF containing 0.4 mL of 1 M TBAF. The mixture was agitated very slowly, and delamination occurred after approximately 1.5 hours. The recovered substrate was removed from the solution, rinsed with acetone, and dried under ambient conditions.

### Anionic ring opening (AROP) of cyclic siloxanes

The clear solution from the depolymerization was concentrated under reduced pressure until a colourless, viscous mixture was obtained. Toluene was added, and the organic phase was extracted with distilled water three times, dried over $Na_2SO_4$, and subsequently filtered. To the remaining solution, a catalytic amount of tetramethylammonium hydroxide was added, and the mixture was stirred for 3 hours at 100 °C. Finally, the polymerization mixture was cooled down to RT and quenched with acetic acid. The product was analysed by size exclusion chromatography (SEC).

### Pencil hardness measurements

Pencil hardness measurements were conducted using an Elcometer 501 pencil hardness tester. Herein, pencils of varying hardness were set at a 45° angle in the Elcometer 501 tool and pushed across the coating surface. The pencils were varied in the following range: 6B, 5B, 4B, 3B, 2B, B, HB, F, H, 2H, 3H, 4H, 5H, 6H, 7H, 8H, and 9H. Afterward, the surface was evaluated for damage using laser-scanning microscopy (LSM). The coating was categorized by "gouge/pencil hardness". Here, the hardness value is determined by whether less than 3 mm of the 6 mm tested surface is cut.

### Contact angle measurements

Contact angle measurements were conducted using a Krüss Drop Shape Analyzer DSA 25E (Krüss GmbH, Germany) on coated microscope glass slides. Here, the volumes of water and diiodomethane droplets were set to 1 µl. The contact angles were determined by the Krüss Advance software (Version 1.19.3.02101) applying the Elipse (Tangente-1)-Fit mode. Herein, the baseline was manually adjusted if necessary. A minimum of five measurements were conducted per sample at different locations, and the average contact angle was calculated.

### Water roll-off angle measurements

The water roll-off angles were analysed by placing a coated glass slide on a tilting stage with manual adjustment of the inclination angle. A droplet of deionized water was deposited onto the coating surface using a glass pipette. Subsequently, the stage was tilted until the droplet began to move across the surface. The mean value of three measurements was calculated for each coating.

### Laser scanning microscopy (LSM)

Laser scanning microscopy images were recorded using a Keyence VK-X200 laser scanning microscope (Keyence Deutschland GmbH, Germany). A 20 times magnification objective was used in combination with the auto-gain and auto-focus function. The surface roughness value $R_a$ was determined using the VK-Analysis software (Version 3.2.0.0). Hereby, the automatic baseline correction tool was used.

### Attenuated total reflectance Fourier-transform infrared (ATR-FTIR) spectroscopy

ATR-FTIR spectroscopy was conducted utilizing a Nicolet iS5 IR spectrometer equipped with a ZnSe crystal from Thermo Fisher Scientific (Waltham, Massachusetts, USA). The OMNIC software was used to evaluate the recorded spectra. Measurement parameters were 16 scans, at a resolution of 0.121 $cm^{-1}$, and a spectral range of 4000 to 400 $cm^{-1}$.

### Thermal gravimetric analysis (TGA)

TGA was conducted by using a NEXTA and STA7200 Thermal Analysis System from Hitachi (Santa Clara, CA, USA). 5–20 mg of sample mass was placed into the ceramic crucible. During a constant airflow of 200 mL $min^{-1}$ the sample was steadily heated with a rate of 10 °C $min^{-1}$ from 25 °C to 1000 °C.

### Scanning electron microscopy-energy-dispersive X-ray spectroscopy (SEM-EDX)

SEM-EDX was performed on the precipitated hybrid residues from the depolymerization trials to investigate their elemental composition. Therefore, we utilized a scanning electron microscope ULTRA 55 (field-emission device, Zeiss, Oberkochen, Germany), which operates with SmartSEM software (Version 5.07). A small portion of the sample was carried on aluminum stubs without additional preparation. The EDX instrument (EDAX, Ametek, USA), which was attached to the

microscope, was used for elemental analysis. The accelerating voltage of the spectra was 5 kV, and the baseline correction as well as the quantification were conducted by utilizing Genesis Spectrum software (Version 6.531).

### $^{29}$Si-nuclear magnetic resonance (NMR) spectroscopy

$^{29}$Silicon NMR spectra were recorded using a Varian INOVA 400 MHz instrument at 79.452 MHz with a spectral width of 19 870 Hz. Tetramethylsilane was used as reference. Spectra for recovered cyclic siloxanes were recorded in $CDCl_3$ at RT, with a 12 s relaxation delay, and 64 scans per sample.

### Size exclusion chromatography (SEC)

SEC measurements were conducted with a SECurity SEC System purchased from PSS Polymer Standards Service GmbH (Mainz, Germany) equipped with a refractive index (RI) and an ultraviolet (UV) detector. Calibration was conducted with polystyrene standards (474 Da to 2 520 000 Da). The eluent was THF at a flow rate of 1 mL min$^{-1}$. The operating temperature was set to 38 °C. Samples with a concentration of approximately 30 mg/100 mg were filtrated over a 0.1 μm syringe filter. Toluene was used as an internal standard. Data were processed with the PSS WinGPC UniChrom software (Version 5).

## Results and discussion

### Recyclable by design: embedding molecular scission points in IOHPCs

Key to the design strategy for recyclable IOHPCs that enables controlled depolymerization and subsequent material recovery is the integration of silicone moieties as molecular scission points within the hybrid matrix, in addition to their conventional roles as flexibility or hydrophobicity enhancers.[44,45]

Scheme 2 illustrates the synthetic approach used to generate the hybrid coating architecture. The formulation combines three silane precursors, namely (3-glycidyloxypropyl)trimethoxysilane (GPTMS), tetraethyl orthosilicate (TEOS), and 3-aminopropyltriethoxysilane (APTES), with linear polydimethylsiloxane (PDMS) chains. In the presence of a tin-based catalyst (dibutyltin dilaurate, DBTL), the silanol-terminated PDMS reacts with silane precursors to covalently integrate the flexible silicone segments into the otherwise rigid hybrid matrix.

To investigate the effects of silicone chain length and concentration on both coating properties and recyclability, several IOHPC formulations were prepared, as shown in Table 1.

IOHPCs were prepared by incorporating either a short silicone chain ($M_w$ of 550 g mol$^{-1}$, S series) or a long silicone chain ($M_w$ of 3400 g mol$^{-1}$, L series), while varying the molar concentrations from 4 to 20 mol% silicone, respectively. Accordingly, samples are referred to as "S_4%" to "S_20%" or as "L_4%" to "L_20%", respectively. The material properties of all model coatings were characterized by hydrophobicity (contact angle measurements) and hardness or scratch resistance (pencil hardness). In addition, the recycling process was performed and evaluated qualitatively as well as quantitatively by analysis of the synthon distribution (ATR-FTIR and $^{29}$Si-NMR spectroscopy). Subsequently, synthon upcycling was performed with a model follow-up reaction. Finally, the integrity of the substrates after delamination was analysed using laser scanning microscopy.

### Functional and tunable: coating properties across formulations

Here, the aim was to design a tunable material that can be adjusted to meet specific application requirements. Therefore, all coating formulations, varying in molecular weight and

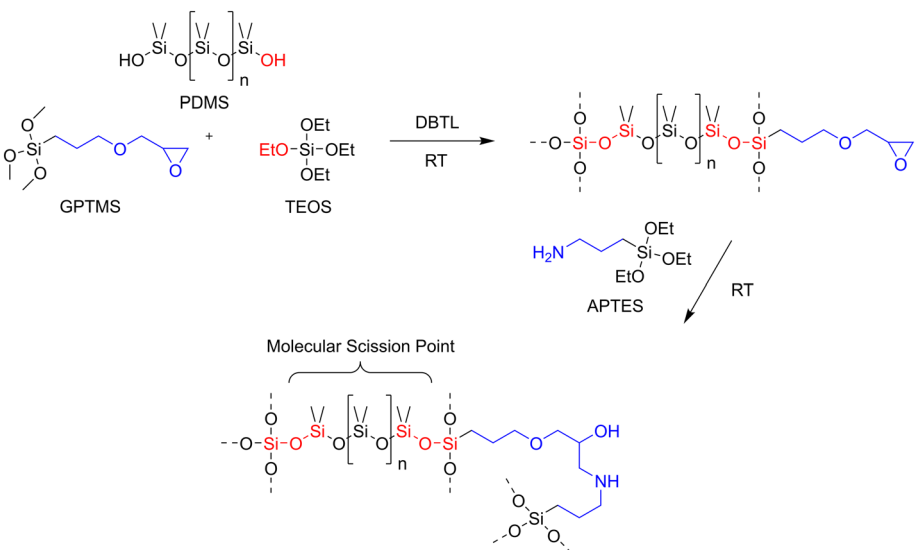


Scheme 2 Synthesis of a recyclable IOHPC. Tetra- and trialkoxysilanes (TEOS, GPTMS and APTES) react with linear, silanol-terminated PDMS at RT using tin catalysis, resulting in siloxane bridges (marked in red). The organic network forms *via* the ring-opening reaction of the epoxy and amino groups of the functional trialkoxysilanes (marked in blue).

 

Table 1 Overview of IOHPC formulations containing short silicone chains of low molecular weight ($M_w$ 550 g mol$^{-1}$, S series) and long silicone chains of higher molecular weight ($M_w$ 3400 g mol$^{-1}$, L series). The ratio of tetra- and trialkoxysilanes remained unchanged

| | | Precursor ratio [mol%] | | | |
|---|---|---|---|---|---|
| Samples | $M_w$ [g mol$^{-1}$] | TEOS | GPTMS | APTES | Silicone |
| S_4% | 550 (short chains, S series) | 32.0 | 32.0 | 32.0 | 4 |
| S_8% | | 30.7 | 30.7 | 30.7 | 8 |
| S_11% | | 29.7 | 29.7 | 29.7 | 11 |
| S_14% | | 28.7 | 28.7 | 28.7 | 14 |
| S_20% | | 26.5 | 26.5 | 26.5 | 20 |
| L_4% | 3400 (long chains, L series) | 32.0 | 32.0 | 32.0 | 4 |
| L_8% | | 30.7 | 30.7 | 30.7 | 8 |
| L_11% | | 29.7 | 29.7 | 29.7 | 11 |
| L_14% | | 28.7 | 28.7 | 28.7 | 14 |
| L_20% | | 26.5 | 26.5 | 26.5 | 20 |

content of the incorporated silicone molecular scission point, were coated onto glass slides and characterized regarding surface hardness by pencil hardness tests and hydrophobicity by water contact angle measurements (exemplary drop shapes are shown in Fig. S1 to S5). These properties can be categorized into two groups: (a) characteristics that remain constant across formulations, and (b) tunable parameters varying in dependency on molecular weight and content of the incorporated silicone. Fig. 1 summarizes both categories showing water contact angles and pencil hardness values. As shown in Fig. 1a the water contact angles of systems S_4% to S_20% exhibit 98°, 96°, 98°, 98°, 95° and systems L_4% to L_20% show 103°, 102°, 101°, 101° and 104°, respectively. Thus, short and long silicone chain-containing systems exhibit nearly constant values across all silicone contents. However, long silicone chain-containing systems exhibit slightly higher water contact angles than the short chain systems, which is in accordance with literature reporting that in this case hydrophobic repeating units tend to be exposed to the surface.[46] Nevertheless, with contact angles ranging from 95° to 104°, the coatings consistently exhibit hydrophobic behaviour due to the presence of methyl groups from the PDMS backbone.[44,47]

This suggests that altering chain lengths or PDMS concentrations within the tested limits does not alter the

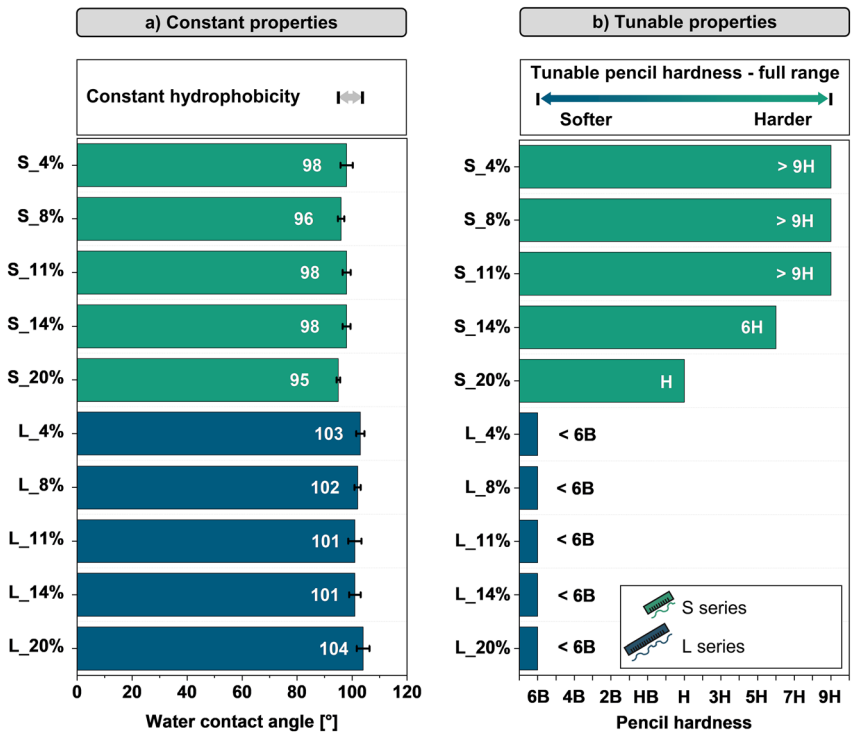


Fig. 1 (a) Displays contact angles against water for constant coating properties across formulations. (b) Shows the tunable pencil hardness in correlation with varying silicone content and different molecular weights of the silicone chains (short silicone chains, S series in green and long silicone chains, L series in blue).

hydrophobicity of the hybrid coating. The same trend holds for contact angles against di-iodomethane and the surface energy, as shown in Table S1. Additionally, the absence of surface segregation and good wettability on different substrates (Fig. S6) at high PDMS loadings (*e.g.*, L_20%) supports the robustness of the coating design.

Furthermore, the prepared coatings show strong parameter dependence regarding the pencil hardness (Fig. 1b). Here, short chain containing coatings S_4% to S_11% showed values of >9H, S_14% of 6H, and S_20% of H, thus exhibiting a decreasing pencil hardness with higher loading. However, long-chain-containing formulations demonstrated pencil hardness values of <6B across the entire concentration range (L_4% to L_20%), corresponding to a very soft character. To understand this trend, it is essential to note that silicone chains contain $Me_2Si–O$ as the repeating unit. This results in a very flexible backbone by allowing easy rearrangement of methyl groups by rotation of the siloxane bond –Si–O–.[48] With this background, the increase in pencil hardness from long to short chains, and from high to low silicone concentrations can be explained by two key factors. First, short chains contain fewer flexible repeating units, resulting in higher pencil hardness. Second, reducing the silicone content in the IOHP formulation reduces the number of flexible units in the polymer matrix, leading to higher pencil hardness values. Additionally, the relative share of rigid crosslinking sites in the matrix is increased. To summarize, the most critical aspect is that tunability across the entire pencil hardness scale, from very hard (9H) to very soft (6B), was achieved.

This shows that the structural matrix design creates a highly versatile coating. It enables precise fine-tuning of coating properties (*e.g.*, pencil hardness) by adjusting a single formulation component: the silicone. At the same time, key surface functionalities, such as hydrophobicity, can be preserved. Thereby, a broad range of applications can be addressed. Those could range from mechanically robust, hydrophobic surfaces on metal substrates to reduce corrosion in the construction sector, thereby eliminating cost and safety risks to very soft, hydrophobic systems bearing potential as erosion protection coatings for wind turbine blades.[49,50]

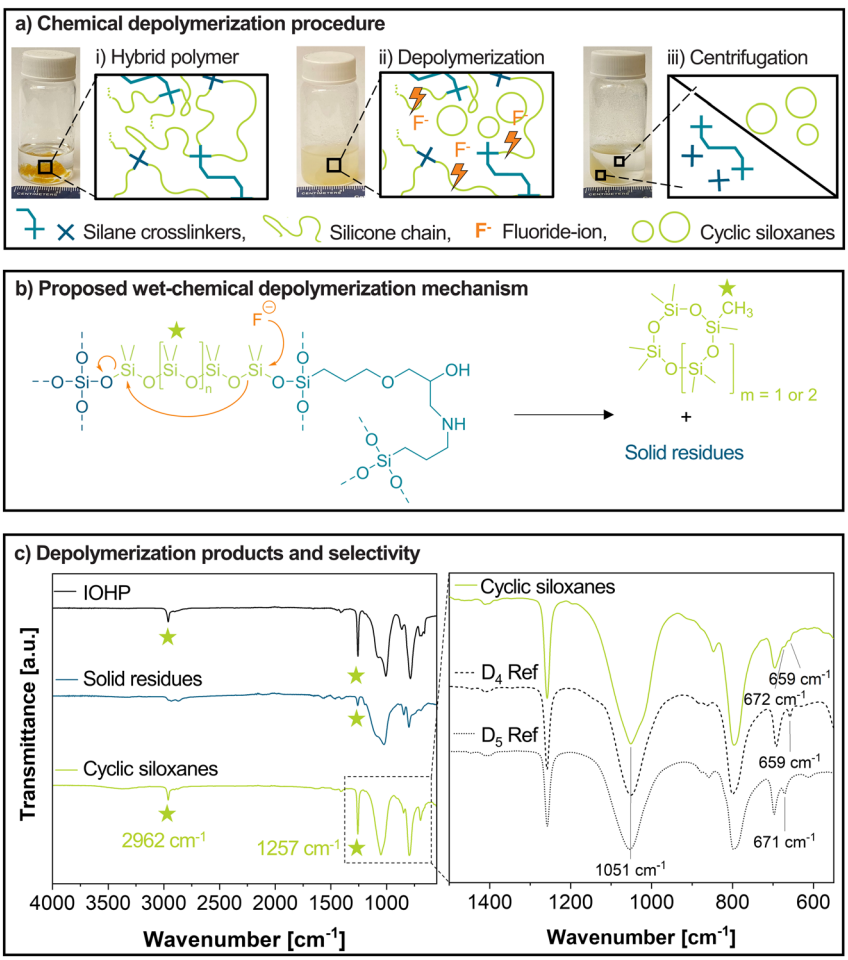


Fig. 2 (a) The depolymerization procedure is, (i) containing the submersion of the IOHP in the depolymerization solution itself, (ii) the depolymerization (iii) and subsequent separation by centrifugation. (b) Proposed, abbreviated wet-chemical depolymerization mechanism based on fluoride-triggered backbiting of PDMS moieties in the hybrid matrix, resulting in cyclic siloxanes and cross-linker residues (note that the full mechanism likely involves pentacoordinated silicon species). (c) ATR-FTIR spectra of the intact IOHP, the isolated residues and the cyclic siloxanes. Here, the $–CH_3$ group (marked with a star) is used as an ATR-FTIR indicator for the selectivity of the depolymerization process.

 

### Triggered depolymerization: selective cleavage inside the hybrid matrix

The objective was to determine whether the collapse of the hybrid matrix could be induced by selective depolymerization of the molecular scission points – the silicone part of the matrix. Therefore, the intact hybrid polymer was subjected to the fluoride-catalyzed depolymerization procedure and analyzed qualitatively and quantitatively (Fig. 2 and 3). For analytical purposes, a bulk sample was used instead of the coating on a surface, and system L_11% was chosen as representative example, because it contains a medium level PDMS concentration within the investigated concentration range. Fig. 2a illustrates the full depolymerization workflow. Initially, the IOHP with its molecular PDMS scission points highlighted in green is submerged in a TBAF-containing EtOAc solution and stirred overnight at RT.

This results into a heterogeneous suspension, visually indicating the collapse of the network structure. Herein, the selective attack of fluoride ions to the silicone scission points (orange flashes in Fig. 2a(ii)) breaks down the silicone chain and results in the depolymerization mixture.[33,34,41] *Via* centrifugation the products can be separated into a solid, non-soluble residue (insoluble cross linkers derived from *e.g.,* GPTES and TEOS) and a clear liquid phase (containing soluble cyclic siloxanes), which is represented in Fig. 2a(iii).

At the structural level, this transformation is illustrated in Fig. 2b. It is postulated that the underlying reaction mechanism is the same as that described in previous publications on silicone rubber recycling: the backbiting mechanism, which likely involves a pentacoordinated silicon species.[34,40,51,52] Herein, a single point of Si–O cleavage is enough to induce degradation of a fully linear polymer, whereas crosslinked networks require more than one starting point.[40] $^{29}$Si-NMR spectroscopy allows direct detection of PDMS depolymerization products in the form of cyclic siloxanes, enabling experimental verification that PDMS chains act as molecular scission points. Here, cyclic oligomers $D_4$, $D_5$ as well as linear residues were present in the recorded $^{29}$Si-NMR spectra (Fig. S7). In this regard, it is literature-known that the formation of cyclic siloxanes derived from the contact of linear PDMS and TBAF occurs *via* the backbiting mechanism.[33,34]

This postulation is additionally supported by ATR-FTIR spectroscopy (Fig. 2c, left side), comparing the spectrum of the intact IOHP, the isolated residues, and the clear solution of the depolymerization mixture. The characteristic signals for the PDMS segment (marked with a star in the solid black curve) at 1257 $cm^{-1}$ (C–H bending vibration of Si–$CH_3$) and at 2962 $cm^{-1}$ (C–H stretching in $CH_3$) nearly disappear in the insoluble residue fraction (blue curve) while being prominently present in the liquid phase (green curve).[53,54] This indicates effective extraction of PDMS segments from the hybrid matrix, likely causing the system to collapse. Two further aspects are worth noting. Firstly, the asymmetric and symmetric Si–O–Si stretching vibrations of the intact IOHP (solid black curve) at 1080 $cm^{-1}$ and 1008 $cm^{-1}$ shift to a narrower signal at 1053 $cm^{-1}$ for the soluble fraction (green curve) after depolymerization.[54] This could be explained by the presence of various silicon species with varying degrees of crosslinking (Q-units from TEOS, T-units from trialkoxysilane, and D-units from PDMS precursors) in the hybrid matrix, compared with fewer silicon species in the soluble fraction. Moreover, SEM-EDX analysis of this insoluble residue fraction indicated the presence of 62 ± 4 at% C, 5 ± 1 at% N, 20 ± 2 at% O, and 16 ± 4 at% Si, corresponding to 50 ± 5 wt% C, 4 ± 0 wt% N, 22 ± 1 wt% O, and 24 ± 4 wt% Si. The TGA measurement (Fig. S8) showed a residual mass of 49 wt% after heat treatment, likely consisting primarily of $SiO_2$. These results further suggest the hybrid character of this residual material. Especially the silicon content bears potential to upcycle this material through additional purification by *e.g.*, silicon-extraction to generate feedstock for silicon-rich filler-type materials.[55,56] However, structural investigation of the residual material remains an important subject for future work. Investigating the ATR-FTIR spectrum of the liquid fraction in more depth and comparing it with cyclic $D_4$ and $D_5$ siloxane references, provides further insights into the nature of the depolymerization products (Fig. 2c, right side). In detail, the spectrum of the

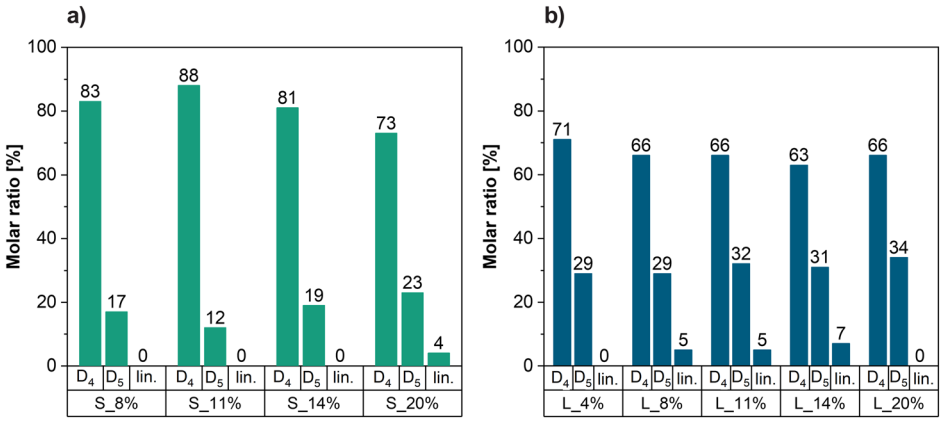


Fig. 3 Molar distribution of siloxane species obtained by depolymerization of IOHPs with molecular PDMS scission points originating from formulations containing (a) short (green, S_8% to S_20%) and (b) long PDMS chains (blue, L_4% to L_20%) after quenching with $CaCl_2$ to remove fluoride ion catalyst.

depolymerization solution showed signals at 672 $cm^{-1}$ and 659 $cm^{-1}$ aligning with the signal of the symmetric stretching of the Si–O–Si group of the $D_5$ reference at 671 $cm^{-1}$ (dotted curve) and of the $D_4$ reference at 659 $cm^{-1}$ (dashed curve), respectively.[54,57]

Additionally, a quantitative study was conducted to gain further insight into the distribution of siloxane products after depolymerization. Generally, cyclic siloxanes are the favoured products of depolymerization over linear residues because they can be reused in industrial silicone synthesis.[33,58] Therefore, all IOHP formulations developed in this work were subjected to the depolymerization process, and the resulting product mixtures were analysed by integrating the corresponding $^{29}Si$ NMR signals at 18.90 ppm, 21.29 ppm, and −21.95 ppm, which correspond to $D_4$, $D_5$, and linear species, respectively (Fig. 3).

As shown in Fig. 3a $D_4/D_5$/linear ratios are 83/17/0 for S_8%, 88/12/0 for S_11%, 81/19/0 for S_14% and 73/23/4 for S_20%, respectively, both quenched with $CaCl_2$ to lock the products from further rearrangements. No NMR signal was observed for S_4%. This could be due to the minimal overall silicone concentration (S_4%) and, thus, of the NMR sample. Fig. 3b displays $D_4/D_5$/linear ratios for long-chain containing systems. Here, ratios are 71/29/0 for L_4%, 66/29/5 for L_8%, 66/32/5 for L_11%, 63/31/7 for L_14% and 66/34/0 for L_20%, respectively. The comparison of short- and long-chain containing systems shows only minor differences. Interestingly, systems S_8% to S_20% exhibit $D_4$ fractions ranging from 88 to 73 mol%, whereas L_4% to L_20% exhibit lower values of 71 to 63 mol%, respectively. At the same time $D_5$ fractions are lower in system S_8% to S_20% (12 to 23 mol%) and higher in L_4% to L_20% (29 to 34 mol%). Also, linear residues are more frequent in long-chain systems, L_8% to L_14%. This may be due to the constant overall polymer-to-EtOAc/TBAF solution ratio. Thus, differences in PDMS content within the polymer matrix resulted in varying effective PDMS/EtOAc and PDMS/TBAF ratios. These differences could account for the observed variations of the depolymerization products.[33] Most importantly, $D_4$ is the dominant depolymerization product across all systems (63–88 mol%), regardless of whether the formulation was prepared with short- or long-chain PDMS and was soft, flexible, or rigid. This finding is particularly significant: it suggests that very different material compositions and architectures yield the same main product. These results highly suggest that the depolymerization proceeds selectively, targeting only the silicone scission points, resulting in $D_4$ as the main product across all investigated formulations, accordingly enabling a universal upcycling route independent of the original coating composition. Also, it is essential to note that the silicone depolymerization process operates under ambient, sustainable conditions, without high temperatures or mechanical impact.

## Closing the loop: upcycling of cyclic siloxanes

The cyclic siloxanes obtained from the depolymerization process were incorporated into ring-opening polymerization (ROP) reactions to validate their principal use as reactants for the synthesis of new silicones (general mechanism shown in Fig. S9). In this regard, ROP was chosen as the model follow-up reaction because it is one of the primary industry pathways for fluid silicone production. The products of this reaction are affected by an extensive range of parameters, such as used initiators (ionic, radical type, peroxide and plasma), monomers ($D_3$, $D_4$, $D_5$ and $D_6$ species), end-capping agents (*e.g.*, disiloxanes), additives and reaction conditions.[58] Herein, we have chosen tetramethylammonium hydroxide (TMAH) as a base initiator for the polymerization of an exemplary $D_4/D_5$-depolymerization mixture (derived from the depolymerization of L_11%), followed by quenching with a vinyl capping agent to ensure defined chain termination. Therefore, reaction conditions based on literature were used, as shown in Scheme 3.[59,60]

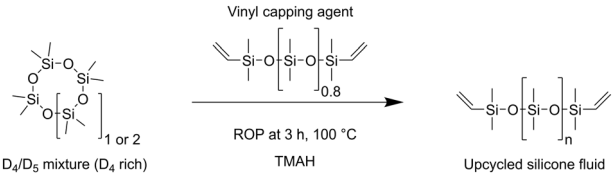


Scheme 3 ROP of a $D_4$-rich depolymerization mixture using tetramethylammonium hydroxide (TMAH) as initiator in the presence of a vinyl capping agent.

The reaction product obtained from ROP was investigated by SEC, as shown in Fig. 4. The neat $D_4$ reference shows a weight-average molecular weight $M_w$ of 538 g $mol^{-1}$ and the vinyl capping agent a $M_w$ of 233 g $mol^{-1}$ (Fig. S10 a and b). However, the chromatogram of the obtained polymerization mixture after performing anionic ROP exhibits a relatively narrow signal with a weight-average molecular weight $M_w$ of 352 g $mol^{-1}$ and a broad signal with a weight-average molecular weight $M_w$ of 1331 g $mol^{-1}$. The first signal is likely due to residual monomers ($D_4$ and $D_5$), whereas the second signal indicates the presence of higher molecular-weight species, suggesting successful repolymerization. The mixture of products observed in the present reaction is a common phenomenon also in the analogue

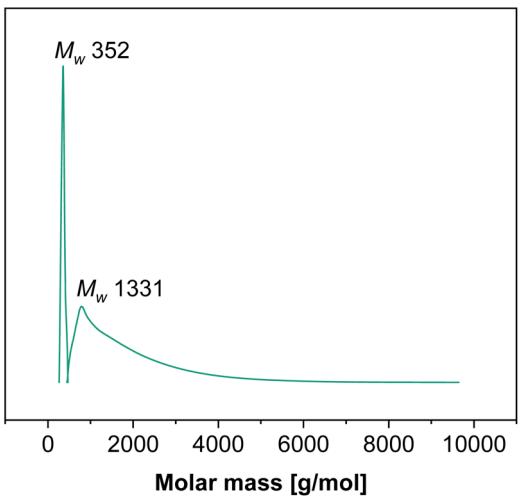


Fig. 4 SEC analysis of the reaction product obtained from the ROP of a $D_4$-rich depolymerization mixture.

industrial synthesis conducted with conventional, non-recycled $D_4$ and $D_5$ feedstock and can be related to the absence of ring strain within $D_4$ and $D_5$ synthons in comparison to $D_3$.[58] This predetermines a thermodynamically controlled reaction pathway, in which the bonds of the monomers and the formed linear polymers are thermodynamically equivalent. Thus, entropy is the main driving force and parallel formation of cyclic and linear PDMS chains occurs, while the polymer formation stops when equilibrium is reached.[58] Further optimization of the ROP was not performed, as it was out of scope for this work. Ensuring the absence of water could lead to a more unimodal product distribution. Herein, vacuum distillation could be utilized for removing the residual volatile components (cyclic siloxanes, capping agent and small linear oligomers) from the upcycled silicone fluid, which is the desired polymerization product.[58,61,62]

To explore the potential reuse of the non-silicone components of the hybrid matrix, we dissolved the recovered solid residue (see Fig. 2a(iii)) in an alkaline solution (pH 14). This solution was subsequently incorporated into the synthesis of literature-known IOHPCs, successfully enabling the production of coatings with up to 4 wt% of these recycled components.[23,63] A comparative analysis with the literature-known reference system showed that key surface properties, such as optical transmission, surface roughness, water contact angle, diiodomethane contact angle, and water roll-off angle, remained nearly unchanged (Fig. S11).[23,63] This demonstrates the chemical compatibility of the non-silicone shares with IOHPCs, which will be explored in more detail in the future.

In conclusion, our ROP investigations show that a $D_4/D_5$ mixture, efficiently recycled from a complex IOHP network at RT, can serve as an adequate feedstock for producing linear PDMS. Especially with respect to the resource intensity of the carbothermal reduction and Müller-Rochow process used to produce chlorosilanes and subsequently cyclic siloxanes, substituting conventional virgin materials with recycled cyclic siloxanes could offer crucial ecological benefits in the future.[40,58]

### Gentle delamination to preserve substrate integrity

The final step in achieving full-loop recycling of IOHPCs, according to the recycling strategy presented here, is the recovery of the substrate. For this purpose, a steel substrate was first coated with L_11% and then delaminated by TBAF-induced depolymerization of incorporated silicone chains acting as molecular scission points. While EtOAc was used for bulk depolymerization trials, THF was employed for coating removal due to more effective delamination. After spontaneous detachment of the coatings after approximately 1 to 1.5 hours, the substrate was rinsed with acetone to remove the depolymerization solution from the surface, investigated by LSM to detect potential surface damages, $SiO_x$ pre-treated, and reused for the next coating cycle. The $SiO_x$ surface pretreatment introduces silanol groups onto the substrate, ensuring consistent surface chemistry across cycles.[64] This prevented changes in adhesion from becoming the limiting factor for the number of delamination cycles. Thus, the experimental design deliberately detects potential surface damage caused by delamination processes rather than the adhesion evolution. This process was repeated over four delamination and subsequent coating cycles (C0–C4), and the results are summarized in Fig. 5a. To distinguish between corrosion caused by the delamination procedure itself and corrosion introduced by ambient exposure, an uncoated reference substrate was investigated in parallel (Fig. 5b). The letter underwent the same pre-treatment and drying steps but was never coated or exposed to the depolymerization solution.

As shown in Fig. 5a, the virgin steel substrates in cycle 0 (C0) exhibit a flawless surface, both the steel substrate to be coated (i) and the reference substrate (ii). After the first delamination cycle (C1, iii to iv), the recovered steel substrate shows no signs of corrosion. However, the corresponding steel reference already exhibits small brown spots (C1, v). After the second delamination cycle, the recovered steel substrate displays the first discolorations (C2, vi to vii), while the steel reference is already majorly corroded (C2, viii). Discolorations of the recovered steel substrate intensify after cycle 3 (C3, ix to x) and remain clearly present after cycle 4 (C4, xii to xiii). In contrast, the reference steel substrate exhibits significant areas of corrosion, which remain at a similar level during cycles 3 and 4 (C3, xi, and C4, xiv). Thus, it is essential to note that the recovered steel substrate never shows more pronounced surface corrosion than the reference steel substrate, indicating that the delamination procedure itself does not harm the substrate. Furthermore, surface changes of the recovered steel substrate appear later in comparison to the reference (C2, vii *vs.* C1, v) and are less pronounced (C2, vii; C3, x; C4, xiii *vs.* C2, viii; C3, xi; C4, xiv) due to the coating's corrosion protection, consequently reducing the steel substrate's contact to ambient air. This is in good agreement with the literature, where PDMS-containing coatings with high water contact angles are frequently used for corrosion protection of metal surfaces.[65–67]

Additionally, surface changes were quantified using the corresponding surface roughness value, $R_a$ (Fig. 5c). Herein, the reference steel substrate shows roughness values $R_a$ of 1.09 μm, 1.23 μm, 1.22 μm, 1.22 μm, and 1.36 μm, respectively, while the recovered steel substrate exhibits $R_a$ values of 1.40 μm, 1.58 μm, 1.39 μm, 1.48 μm, and 1.37 μm, respectively, from cycle C0 to C4. Thus, the increase in surface roughness is less pronounced for the recovered steel substrate than for the reference steel substrate, related to the coating's corrosion protection, additionally indicating a gentle coating release. Accordingly, we investigated the extent of delaminations of the IOHPC containing molecular silicone scission points on different substrates. Thus, a gentle release was possible for glass, polyolefin, and aluminum (Fig. S12–S14) validating the mild coating delamination process (RT, no abrasion or mechanical stress) consequently allowing not only the reuse of IOHP coating components, but also the recovery of valuable substrate materials.

In this study, we prioritized comparability across the different substrate trials and thus conservatively fixed the delamination time to 1.5 h, avoiding substrate-dependent delamination times. These conditions guaranteed total

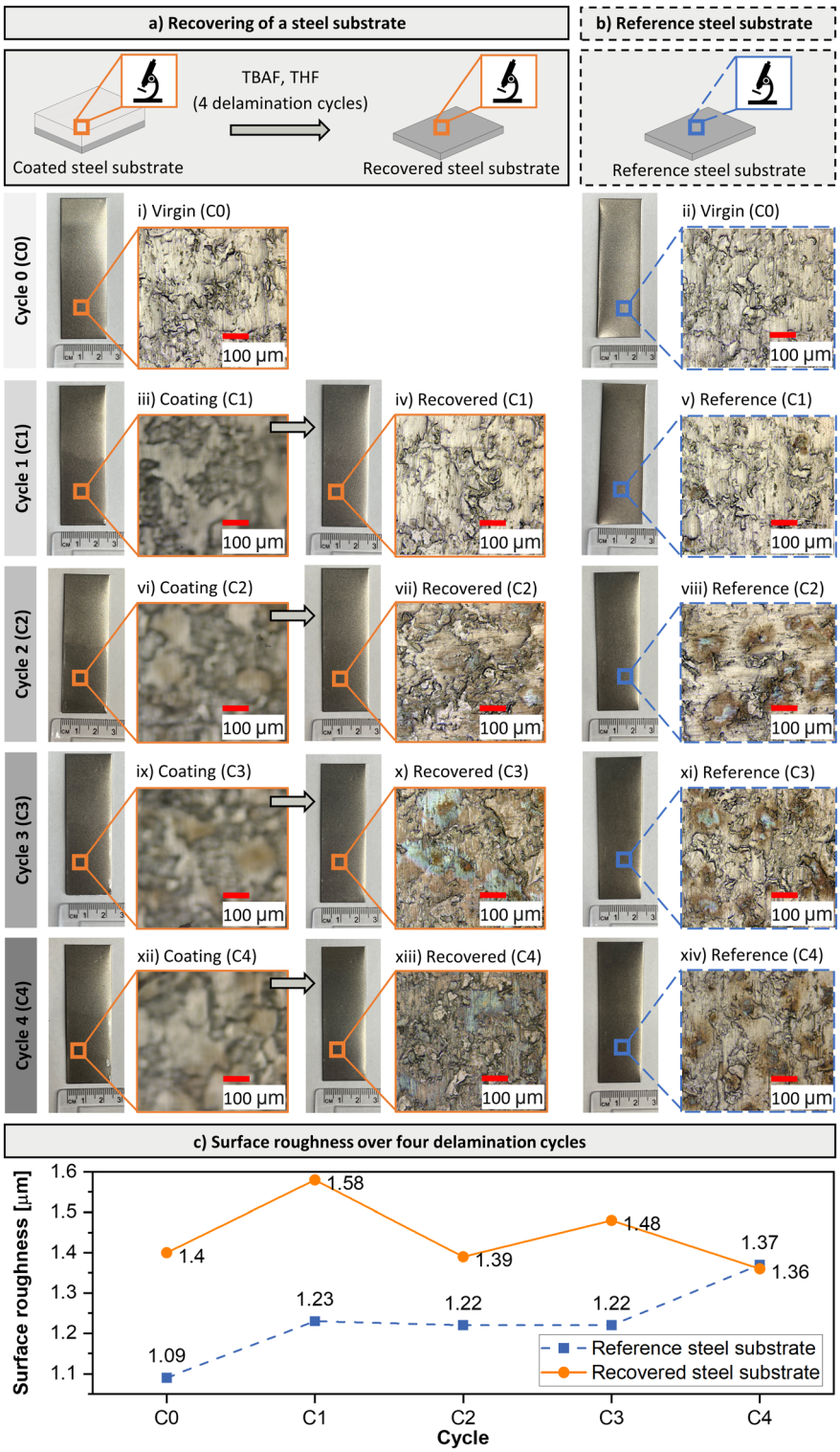


Fig. 5 (a) Recovering of the coated steel substrate by delamination with a depolymerization solution (THF/TBAF). Surface changes were evaluated *via* laser scanning microscopy. In the LSM images of the coated steel substrate, focus was set on the coating surface. Since the coating is transparent, the underlying substrate appears blurred. (b) An uncoated steel reference substrate was analysed in parallel to investigate corrosion traces occurring over the storage time introduced by ambient exposure. (c) The evolution of the surface roughness values ($R_a$) is displayed for the recovered and the reference steel substrate.

delamination without further mechanical force in each case. However, the minimum required delamination times may reflect a combination of the PDMS rearrangement kinetic, transport processes of the fluoride into the hybrid matrix, solvent swelling, and substrate-dependent binding to IOHPCs.[33,34] Therefore, future studies will aim for the process

 

optimization by tuning the fluoride concentration, the type of catalyst, the reaction temperature, the solvent system and by introducing mechanical impact. This is important to assess the industrial scale up of this concept.

## Conclusions

This study demonstrated the successful molecular redesign of recyclable IOHPCs by integrating silicone scission points while maintaining coating performance. The preservation of functional coating performance was demonstrated by hydrophobic surfaces (water contact angles of 95° to 104°) and tunable pencil hardness ranging from very soft to very hard (6B to 9H) with varying silicone chain length and concentration. Upon contact with the TBAF catalyst, the hybrid matrix collapsed, and the IOHPC delaminated from the substrate without mechanical force, confirming the fluoride-triggered decomposition. This yielded valuable products in the form of cyclic siloxanes, with $D_4$ as the main product (>63%) across all IOHPC formulations, serving as feedstock for silicone synthesis. Additionally, the recovered substrates were undamaged and could be recoated directly, confirming the circularity of the process. Notably, this research fundamentally reinterpreted the role of silicones in the IOHPC chemistry, using them as scission points rather than merely as hydrophobicity or flexibility enhancers. Future studies will explore different bonding types as potential scission points to enable compatibility with further recycling processes. In general, adopting a design-for-recycling approach at the molecular scale in IOHPCs demonstrates how performance and circularity can be combined effectively, thereby contributing to a sustainable future.

## Ulrich Schubert dedication

This manuscript is dedicated to the lifetime of achievement, progress, and inspiration of Ulrich Schubert in the field of *Sol-Gel Science*.

## Author contributions

C. F. conceived the study, designed, and performed the experiments, carried out the formal analysis, and wrote the original manuscript draft. J. C. F. supervised the work and contributed to the experimental design and manuscript revision. A. H., F. S., C. S., D. L., and G. S. assisted with data acquisition and contributed to discussions and manuscript review. All authors contributed to the writing, review and editing and approved the final version of the manuscript.

## Conflicts of interest

The authors declare no conflict of interest.

## Data availability

All data supporting the findings of this study are available within the article and its supplementary information (SI). Additional raw data or materials can be provided by the corresponding author upon reasonable request. Supplementary information: contact angles against water as well as $CH_2I_2$ and surface energy values for every coating system, images of coloured coatings on different substrates, $^{29}$Si-NMR data of the soluble fraction of the depolymerization mixture, a general reaction scheme of anionic ROP, an overview of the reuse of non-silicone matrix shares, LSM analysis of a delaminated microscope glass slide, images of the delamination process of different substrates, and an overview of the general coating delamination process, SEC data of a neat $D_4$ sample, the neat vinyl-capping agent and the repolymerized PDMS. See DOI: https://doi.org/10.1039/d6ta00284f.

## Acknowledgements

The authors gratefully acknowledge Ethan Chandler and Andrew Deller for the invaluable guidance and support during performing the laboratory work. This research was supported by the Evonik Foundation by a doctoral scholarship to C. F. and Bowling Green State University Startup Funding. The cooperation was funded by the Fraunhofer International Mobility Program.

## References

1 K. Houssini, J. Li and Q. Tan, *Commun. Earth Environ.*, 2025, **6**, 257.
2 Y. Weng, C.-B. Hong, Y. Zhang and H. Liu, *Green Chem.*, 2024, **26**, 571–592.
3 S. Yang, S. Du, J. Zhu and S. Ma, *Chem. Soc. Rev.*, 2024, **53**, 9609–9651.
4 H. Mangold and B. von Vacano, *Macromol. Chem. Phys.*, 2022, **223**, 2100488.
5 O. Horodytska, F. J. Valdés and A. Fullana, *Waste Manag.*, 2018, **77**, 413–425.
6 I. A. Ignatyev, W. Thielemans and B. Vander Beke, *ChemSusChem*, 2014, **7**, 1579–1593.
7 C. T. M. Soares, M. Ek, E. Östmark, M. Gällstedt and S. Karlsson, *Resour. Conserv. Recycl.*, 2022, **176**, 105905.
8 V. Lahtela, S. Silwal and T. Kärki, *Polymers*, 2020, **12**, 2517.
9 M. Y. Khalid, Z. U. Arif, W. Ahmed and H. Arshad, *Sustain. Mater. Technol.*, 2022, **31**, e00382.
10 P. H. Shipway, J. Bromley and D. P. Weston, *Wear*, 2007, **263**, 309–317.
11 T. W. Walker, N. Frelka, Z. Shen, A. K. Chew, J. Banick, S. Grey, M. S. Kim, J. A. Dumesic, R. C. van Lehn and G. W. Huber, *Sci. Adv.*, 2020, **6**, eaba7599.
12 E. Bescher and J. D. Mackenzie, *J. Sol-Gel Sci. Technol.*, 2003, **26**, 1223–1226.
13 M. Ghodrati, M. Mousavi-Kamazani and Z. Bahrami, *Sci. Rep.*, 2023, **13**, 548.
14 *Handbook of Sol-Gel Science and Technology*, ed. L. Klein, M. Aparicio and A. Jitianu, Springer International Publishing, Cham, 2016.
15 M. Talha, Y. Ma, M. Xu, Q. Wang, Y. Lin and X. Kong, *Ind. Eng. Chem. Res.*, 2020, **59**, 19840–19857.

16 C. Fischer, H. Bleicher, D. Lau, C. Stauch, G. Sextl and F. Somorowsky, *ACS Sustain. Chem. Eng.*, 2025, **13**, 18544–18555.
17 M. Pilz and H. Römich, *J. Sol-Gel Sci. Technol.*, 1997, **8**, 1071–1075.
18 P. Gomez-Romero, A. Pokhriyal, D. Rueda-García, L. N. Bengoa and R. M. González-Gil, *Chem. Mater.*, 2024, **36**, 8–27.
19 K.-H. Haas and K. Rose, *Adv. Mater.*, 2003, **5**, 47–52.
20 F. Mammeri, E. Le Bourhis, L. Rozes and C. Sanchez, *J. Mater. Chem.*, 2005, **15**, 3787–3811.
21 J. Jang, H. J. Kwon, K.-S. Hwang and J.-Y. Lee, *Adv. Mater. Technol.*, 2024, **9**, 2400383.
22 K.-H. Haas and H. Wolter, *Curr. Opin. Solid State Mater. Sci.*, 1999, **4**, 571–580.
23 K. Emmert, S. Amberg-Schwab, F. Braca, A. Bazzichi, A. Cecchi and F. Somorowsky, *Polymers*, 2021, **13**, 1257.
24 G. Venkatesh, Å. Nyflött, C. Bonnerup and M. Lestelius, *Environ. Dev. Sustain.*, 2018, **20**, 1483–1497.
25 T. Tomše, P. Kubelka, R. Moreno López, P. Fleissner, L. Grau, M. Zaplotnik and C. Burkhardt, *Materials*, 2024, **17**, 5927.
26 L. Grau, P. Fleissner, S. Kobe and C. Burkhardt, *Materials*, 2024, **17**, 2487.
27 V. Ventosinos Louzao, D. García Murias, M. Á. de Dios Álvarez, P. A. Acuña Domínguez, E. Paredes Barros and R. Ledo Bañobre, *Open Res. Eur.*, 2025, **4**, 51.
28 H. Geist and F. Balle, *J. Ind. Ecol.*, 2025, **29**, 1505–1522.
29 D. J. Osborne and P. W. Morgan, *Crit. Rev. Plant Sci.*, 1989, **8**, 103–129.
30 H. Liu, H. Li, G. Yang, G. Yuan, Y. Ma and T. Zhang, *Postharvest Biol. Technol.*, 2021, **172**, 111380.
31 Q. Ding and H. Zhu, *Polymers*, 2023, **15**, 1485.
32 B. von Vacano, H. Mangold, G. W. M. Vandermeulen, G. Battagliarin, M. Hofmann, J. Bean and A. Künkel, *Angew. Chem., Int. Ed.*, 2023, **62**, e202210823.
33 A. C. Deller, H. E. Armenta, E. A. K. D. Edirisinghe, M. E. Deller, K. L. Major, B. Rupasinghe and J. C. Furgal, *RSC Sustain.*, 2025, **3**, 4776–4784.
34 B. Rupasinghe and J. Furgal, *ACS Appl. Polym. Mater.*, 2021, **3**, 1828–1839.
35 N. D. Vu, A. Boulègue-Mondière, N. Durand, J. Raynaud and V. Monteil, *Green Chem.*, 2023, **25**, 3869–3877.
36 M. J. Warner, J. W. Kopatz, D. P. Schafer, J. Kustas, P. S. Sawyer, A. M. Grillet, B. H. Jones and K. Ghosh, *Chem. Commun.*, 2024, **60**, 1188–1191.
37 N. Đ. Vũ, A. Boulegue-Mondière, N. Durand, J. Munsch, M. Boste, R. Lhermet, D. Gajan, A. Baudouin, S. Roldán-Gómez, M.-E. L. Perrin, V. Monteil and J. Raynaud, *Science*, 2025, **388**, 392–400.
38 E. O. Minyaylo, A. I. Kudryavtseva, M. N. Temnikov, A. S. Peregudov, A. A. Anisimov and A. M. Muzafarov, *React. Chem. Eng.*, 2025, **10**, 922–930.
39 A. T. Wolf and A. Stammer, *Polymers*, 2024, **16**, 2220.
40 B. Rupasinghe and J. C. Furgal, *Polym. Int.*, 2022, **71**, 521–531.
41 D. J. Krug, M. Z. Asuncion and R. M. Laine, *ACS Omega*, 2019, **4**, 3782–3789.
42 E. A. Cherney and R. S. Gorur, *IEEE Trans. Dielectr. Electr. Insul.*, 1999, **6**, 605–611.
43 F. Basquiroto de Souza, J. Bautista, A. Giam, C. W. Wong and S. D. Pang, *Polym. Degrad. Stab.*, 2025, **236**, 111299.
44 M. M. Stanton, R. E. Ducker, J. C. MacDonald, C. R. Lambert and W. Grant McGimpsey, *J. Colloid Interface Sci.*, 2012, **367**, 502–508.
45 C. Sanchez, B. Julián, P. Belleville and M. Popall, *J. Mater. Chem.*, 2005, **15**, 3559–3592.
46 T. Zhou, B. Wang, X. Wang, H. Sun, Y. Liu and L. Zheng, *ACS Sustain. Chem. Eng.*, 2023, **11**, 15397–15409.
47 K.-Y. Law, *J. Phys. Chem. Lett.*, 2014, **5**, 686–688.
48 M. P. Wolf, G. B. Salieb-Beugelaar and P. Hunziker, *Prog. Polym. Sci.*, 2018, **83**, 97–134.
49 L. Ejenstam, PhD thesis, KTH Royal Institute of Technology, 2015.
50 J. Wang, M. Yin, C. Yu, S. Tu and J. Feng, *Prog. Org. Coat.*, 2025, **200**, 109013.
51 N. Grassie and I. G. Macfarlane, *Eur. Polym. J.*, 1978, **14**, 875–884.
52 R. C. Osthoff, A. M. Bueche and W. T. Grubb, *J. Am. Chem. Soc.*, 1954, **76**, 4659–4663.
53 F. Ji, P. Fu, S. Wang, T. Liu, L. Lv, X. Guan, X. Zhang, H. Zhao, X. Qiao, X. Pang, M. Liu, Q. Zhao and Z. Cui, *React. Funct. Polym.*, 2020, **154**, 104688.
54 J. Lancastre, N. Fernandes, F. Margaça, I. M. Miranda Salvado, L. M. Ferreira, A. N. Falcão and M. H. Casimiro, *Radiat. Phys. Chem.*, 2012, **81**, 1336–1340.
55 J. Furgal and C. Lenora, *Phys. Sci. Rev.*, 2019, **5**, 20190024.
56 M. Borzova, F. Gauvin and K. Schollbach, *ACS Sustain. Chem. Eng.*, 2025, **13**, 2955–2965.
57 L. Sigot, G. Ducom and P. Germain, *Micropor. Mesopor. Mat.*, 2015, **213**, 118–124.
58 T. Köhler, A. Gutacker and E. Mejía, *Org. Chem. Front.*, 2020, **7**, 4108–4120.
59 X. Li, R. Yu, T. Zhao, Y. Zhang, X. Yang, X. Zhao and W. Huang, *Eur. Polym. J.*, 2018, **108**, 399–405.
60 C. Yu, K. Shi, J. Ning, Z. Zheng, H. Yu, Z. Yang and J. Liu, *Polymers*, 2021, **13**, 2980.
61 G. Ducom, B. Laubie, C. Chottier, P. Germain and V. Chatain, *Water Sci. Technol.*, 2013, **68**, 813–820.
62 B. Yactine, A. Ratsimihety and F. Ganachaud, *Polym. Adv. Technol.*, 2010, **21**, 139–149.
63 K.-H. Haas, S. Amberg-Schwab, K. Rose and G. Schottner, *Surf. Coat. Technol.*, 1999, **111**, 72–79.
64 H. Hillborg, J. F. Ankner, U. W. Gedde, G. D. Smith, H. K. Yasuda and K. Wikström, *Polymer*, 2000, **41**, 6851–6863.
65 L. Ejenstam, A. Swerin, J. Pan and P. M. Claesson, *Corros. Sci.*, 2015, **99**, 89–97.
66 X. Cui, G. Zhu, Y. Pan, Q. Shao, C. Zhao, M. Dong, Y. Zhang and Z. Guo, *Polymer*, 2018, **138**, 203–210.
67 X. Sun, J. Xie, J. Zhang, M. Sang, Y. Li, P. Lyu, D. Chen and H. Zhou, *J. Inorg. Organomet. Polym. Mater.*, 2022, **32**, 4237–4249.

 